JACS
JOURNAL OF THE AMERICAN CHEMICAL SOCIETY

Article

Sulfur-Based Intramolecular Hydrogen-Bond: Excited-State Hydrogen-Bond On/Off Switch with Dual Room-Temperature Phosphorescence

Zong-Ying Liu, Jiun-Wei Hu, Chun-Hao Huang, Teng-Hsing Huang, Deng-Gao Chen, Ssu-Yu Ho, Kew-Yu Chen, Elise Y. Li, and Pi-Tai Chou

J. Am. Chem. Soc., **Just Accepted Manuscript** • DOI: 10.1021/jacs.9b02765 • Publication Date (Web): 05 Jun 2019

Just Accepted

is published by the American Chemical Society. 1155 Sixteenth Street N.W., Washington, DC 20036

Sulfur-Based Intramolecular Hydrogen-Bond: Excited-State Hydrogen-Bond On/Off Switch with Dual Room-Temperature Phosphorescence

Zong-Ying Liu,[†,¶] Jiun-Wei Hu,[‡,¶] Chun-Hao Huang,[§,¶] Teng-Hsing Huang,[‡] Deng-Gao Chen,[†] Ssu-Yu Ho,[†] Kew-Yu Chen,[‡*] Elise Y. Li,[§*] Pi-Tai Chou[†*]

[†]Department of Chemistry, National Taiwan University, Taipei, 10617, Taiwan, R.O.C.

[‡]Department of Chemical Engineering, Feng Chia University, Taichung, 40724, Taiwan, R.O.C.

[§]Department of Chemistry, National Taiwan Normal University, Taipei, 11677, Taiwan, R.O.C.

[¶]These three authors contributed equally

KEYWORDS: Thiones, sulfur hydrogen bonds, hydrogen bond switch, room-temperature phosphorescence

ABSTRACT: We report O-H----S hydrogen-bond (H-bond) formation and its excited-state intramolecular H-bond on/off reaction unveiled by room-temperature phosphorescence (RTP). In this seminal work, this phenomenon is demonstrated with 7-hydroxy-2,2-dimethyl-2,3-dihydro-1*H*-indene-1-thione (**DM-7HIT**), which possesses a strong polar (hydroxy)-dispersive (thione) type H-bond. Upon excitation, **DM-7HIT** exhibits anomalous dual RTP with maxima at 550 and 685 nm. This study found that the lowest lying excited state (S_1) of **DM-7HIT** is a sulfur non-bonding (n) to π* transition, which undergoes O-H bond flipping from $S_1(n\pi^*)$ to the non-H-bonded $S'_1(n\pi^*)$ state, followed by intersystem crossing and internal conversion to populate the $T'_1(n\pi^*)$ state. Fast H-bond on/off switching then takes place between $T'_1(n\pi^*)$ and $T_1(n\pi^*)$, forming a pre-equilibrium that affords both the $T'_1(n\pi^*$, 685 nm) and $T_1(n\pi^*$, 550 nm) RTP. The generality of the sulfur H-bond on/off switching mechanism, dubbed a molecule wiper, was rigorously evaluated with a variety of other H-bonded thiones, and these results open a new chapter in the chemistry of hydrogen bonds.

INTRODUCTION

Hydrogen bonds (H-bonds) typically involve a combination of an O-H or an N–H proton donor and an N or an O proton acceptor, and the corresponding energies can be in a range of several to ten kcal/mol, depending on the H-bond geometry and distance. There have been interesting but few reports on H-bonds that involve a sulfur atom as either the proton donor (S-H) or acceptor (S). The concept of "sulfur participating in an H-bond" appeared in early reports despite the relatively low electronegativity (2.58) for sulfur on the Pauling scale.[1-3] Recent quantum chemical calculations in conjunction with high-resolution spectroscopic evidence has revealed that sulfur-containing H-bond can be as strong as conventional H-bonds.[4-7] In biological systems, methionine-containing dipeptides have been reported to form amide-N–H···S intermolecular H-bonds that are stronger than amide-N–H···O=C H-bonds.[8] Additionally, the strength of the intermolecular H-bonds in thiobase pairs are reported to be of the same magnitude with the canonical nucleobase pairs.[9] As a result, the intermolecular sulfur H-bonds play an important role in artificial DNA or RNA researches[10] and have been applied to RNAi resistant genes[11] and protein engineering.[12] From the viewpoint of applications, Aida and co-workers recently constructed flexible intermolecular N-H···S H-bonds with thiourea units in a polymer backbone and successfully demonstrated their unique ability to heal ruptured polymers at ambient temperature.[13] In particular, sulfur is not only a potential H-bond acceptor, but the S–H group is also a very good H-bond donor and can form a variety of H-bonds. For example, the S–H···π intermolecular H-bond between H_2S and indole/benzene was found to be stronger than O–H···π, O–H···π, and C–H···π H-bonds.[14-16]

Apart from the intermolecular H-bond, the intramolecular sulfur H-bonds have also attracted considerable attention.[17-20] In biological systems, the structure as well as the nature of proteins are often determined by intramolecular sulfur H-bonds. Despite the ubiquity of intramolecular sulfur H-bonds, explorations of their photophysical properties, which help understand the fundamentals of protein folding, conformation and function,[21] remain rather scarce.[22-25]

One of the most intriguing photophysical properties associated with H-bonds can be attributed to the proton-transfer phenomenon, particularly excited-state intramolecular proton transfer (ESIPT), which has been widely studied for more than six decades.[26-29] In this context, through the existing intramolecular H-bonds, ESIPT involves the transfer of a proton from O-H or N–H proton donors to =O or N proton acceptors, forming an excited-state proton-transfer tautomer that does not exist in the ground state. Accordingly, the anomalously large Stokes shift of the emission of the tautomer allows a variety of applications such as in sensing,[30-33] bio-imaging,[34-35] organic lasing[36-38] and light-emitting diodes.[37, 39-41] Such an O-H (N-H)----N (or O) ESIPT occurs in a static dipole-dipole-type H-bond where both the proton-donating and the

Scheme 1. Overview of the synthetic routes to the title thione compounds. Inset: Displacement ellipsoid representation of 7HIT with the atoms labelled. The ellipsoids are drawn at the 50% probability level, and the H atoms are drawn as spheres of arbitrary radii. The blue dashed line denotes the intramolecular O-H---S hydrogen bond.

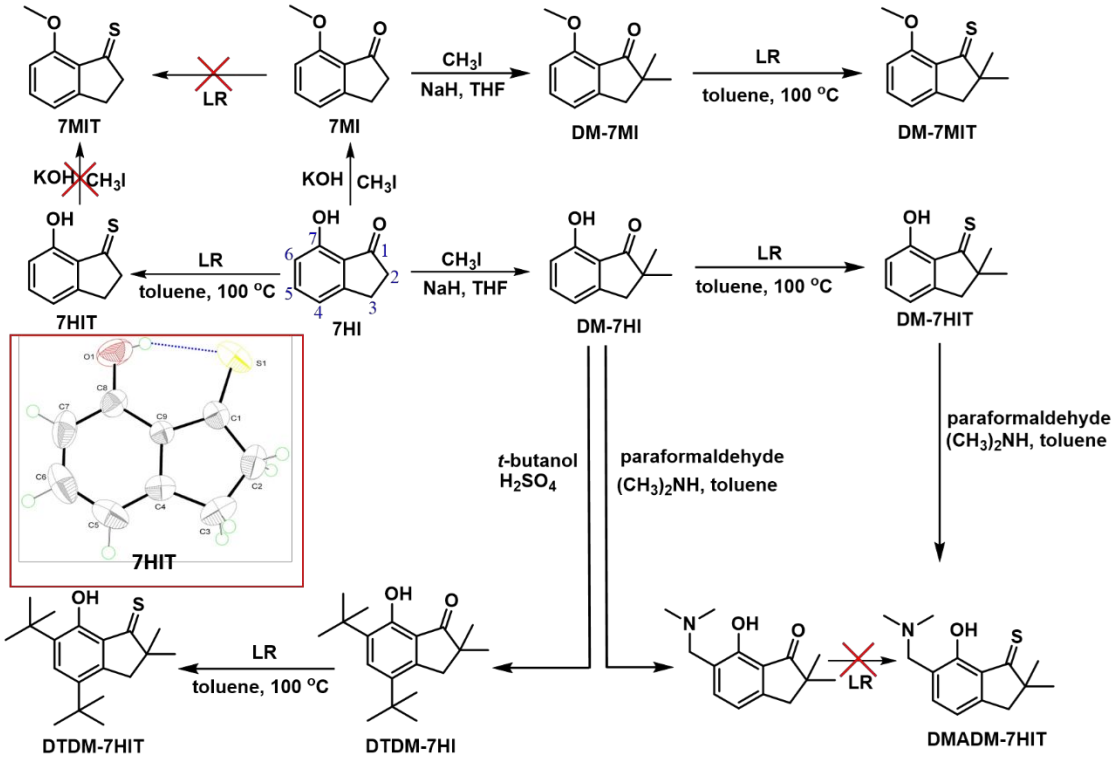

proton-accepting atoms have large electronegativities (> 3.5) on the Pauling scale. In contrast, H-bonds involving S-H (donor) or S (acceptor) are a result of their inherent dispersivity. If ESIPT takes place via the sulfur H-bond, fundamentally, the properties of its potential energy surface and hence its dynamics should be unlike those of ESIPT involving conventional Pauling-type H-bonds. On the other hand, if ESIPT is prohibited, determining the factors controlling the fate of the excited-state relaxation pathway of molecules containing intramolecular sulfur H-bonds would be of fundamental importance. To the best of our knowledge, no theoretical or experimental approaches have addressed proton transfer and/or other distinct photophysical properties of sulfur-containing intramolecular H-bonds. Using 7-hydroxy-2,2-dimethyl-2,3-dihydro-1*H*-indene-1-thione (**DM-7HIT**) as the model system, herein, we report a study on intramolecular O-H----S H-bond formation and the remarkable excited-state behaviour of these bonds, i.e., the photoinduced intramolecular H-bond on/off switching reaction. The mechanism was confirmed and its generality was rigorously tested using a series of new compounds with strategically placed H-bonded and non-H-bonded thiones (see **Scheme 1**).

RESULTS AND DISCUSSION

Synthesis and characterization All the thiones were synthesized via sulfurization of their corresponding carbonyl compounds using Lawesson's reagent (**Scheme 1**).[42-43] The details of synthetic route and product characterization data are presented in the Supporting Information (**SI**). Notably, **7HIT**, depicted in **Scheme 1**, is structurally simpler than **DM-7HIT**, but its photophysical properties are nearly identical to those of **DM-7HIT** (*vide infra*). Unfortunately, attempts towards the *O*-methylation of **7HIT** to form the non-H-bonded model system (**7MIT**) as a reference failed due to decomposition of the thiocarbonyl group. On the other hand, direct thionation of 7-methoxy-2,3-dihydro-1*H*-inden-1-one (**7MI**, see **Figure S3** for X-ray structure) with Lawesson's reagent underwent an unexpected cyclization reaction at the C2 position[44] (see **Scheme 1** for the numbering of the atoms). This cyclization reaction is inhibited by dimethyl substitution at the C2 position, as seen in **DM-7HI** and **DM-7MI** (see **Figure S4** for X-ray structure); as a result, **DM-7MIT**, the non-H-bonded reference for **DM-7HIT**, can be synthesized. Therefore, **DM-7HIT** was used as the prototype throughout this study. Attempts to synthesize **DMADM-7HIT** from **DM-7HI** followed by a Mannich reaction and treatment with Lawesson′s reagent failed due to the reactive Lawesson′s reagent attacking the amino group. Instead, **DMADM-7HIT** was synthesized from **DM-7HI** by treatment with Lawesson′s reagent prior to the Mannich reaction (**Scheme 1**). As shown in **Figure S14, S18, S20,** and **S22**, the ^{1}H NMR spectra of **DM-7HIT** and the other hydroxyl-thiones reported to have sulfur-containing intramolecular H-bonds (**DTDM-7HIT**, **DMADM-7HIT** and **7HIT**) all show dramatically downfield shifted phenolic –OH protons at >9.0 ppm, suggesting a very electron-deficient proton. Interestingly, despite **7HIT** being a solid (melting point 75-76 °C), **DM-7HIT** has a melting point of approximately 10 °C and thus is a liquid at room temperature. Therefore, a single crystal of **7HIT** was obtained and used as a model for structural elucidation. **Scheme**

1 shows the labelled ellipsoid representation of **7HIT**. The O–H···S distance, which is artificially drawn as a blue dashed

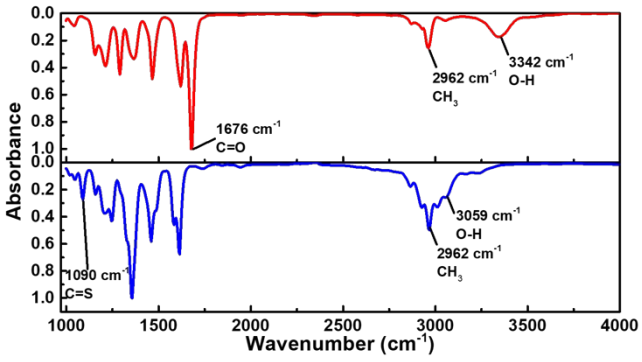

Figure 1. The mid-IR spectra of **DM-7HI** (red) and **DM-7HIT** (blue) at room temperature.

line, was calculated to be 2.2 Å with an ∠O–H···S angle of 152°, making it nearly coplanar with the main chromophore. The short O-H···S distances, along with the coplanar conformation, implies the high possibility of formation of intramolecular O-H···S H-bond.

To check the above conjecture, we then carried out the Fourier transform infrared spectrum measurement for **DM-7HIT** and **DM-7HI**, the latter acts as a comparison (**Figure 1**). The mid-IR spectrum of **DM-7HI** shows a broad absorption band peaked at 3342 cm^{-1}, which can be assigned to the H-bonded O-H stretching. The absorption band at 1676 cm^{-1} for **DM-7HI** can be ascribed as the C=O stretching. On the other hand, the mid-IR spectra of **DM-7HIT** drastically changes upon substitution of sulfur for carbonyl oxygen. The C=O stretching observed in **DM-7HI** vanishes; instead, a sharp absorption band can be resolved at 1090 cm^{-1}, which can be assigned to C=S stretching signal.[45] Another difference is the disappearance of the broad O-H stretching signal at 3342 cm^{-1}; instead, a broad absorption band can be observed at about 3059 cm^{-1}, which overlaps with C-H asymmetric stretching signal (2962 cm^{-1}). In addition, the deuteration of hydroxyl group was conducted, forming **DM-7DIT**, for comparison and the result is shown in **Figure S26**. Clearly, the broad band at 3059 cm^{-1} (**DM-7HIT**) shifts to 2285 cm^{-1} (**DM-7DIT**), reaffirming that the broad 3059 cm^{-1} signal is attributed to the O-H stretching motion. Remarkably, the O-H stretching frequency for **DM-7HIT** is lower than that for **DM-7HI**, which proves the formation of a stronger intramolecular H-bond than **DM-7HI**.

To provide further support for H-bond formation, the cyclic voltammograms (CV) for **DM-7HIT** and **DM-7MIT** are also carried out (**Figure S27**). Both **DM-7HIT** and **DM-7MIT** undergo irreversible one-electron oxidation and reduction, the oxidative and reductive potentials are recorded at 1.67 and -1.81 V (versus $Ag/AgNO_3$ electrode) for **DM-7HIT**, and 1.32 and -1.98 V (versus $Ag/AgNO_3$ electrode) for **DM-7MIT**, respectively. Remarkably, both the first oxidative and the first reductive potentials of **DM-7MIT** are shifted toward more negative values compared with **DM-7HIT**, which indicate that the removal of electrons from **DM-7HIT** is more arduous than that of **DM-7MIT**. According to the previous reports, the HOMO of these thione compounds are the nonbonding orbital of the sulfur atom (*vide infra*).[46-49] Hence, the results reaffirm intramolecular H-bonding formation in **DM-7HIT** that stabilizes the HOMO (nonbonding orbital). Furthermore, the lower HOMO energy level (-6.19 eV) of **DM-7HIT** than that of **DM-7MIT** (-5.84 eV), calculated by CV measurement, also supports the above statement.

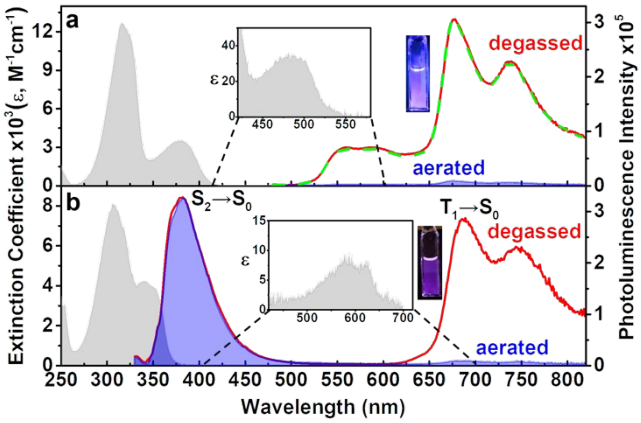

Figure 2. a, Absorption (grey filled area) and emission spectra (blue filled area and solid red line) of **DM-7HI** in cyclohexane at room temperature. The green dashed line represents the emission spectrum of **DM-7DIT**. **b**, Absorption (grey filled area) and emission spectra (blue filled area and solid red line) of **DM-7MIT** in cyclohexane at room temperature. Insets: Expansions of the absorption spectra over specified wavelength regions. λ_{ex}: 380 and 350 nm for **DM-7HIT** and **DM-7MIT**, respectively. Note that the labelling "aerated" refers to aeration in atmosphere.

Spectroscopy and Dynamics The absorption and emission spectra of **DM-7HIT**, **DM-7DIT** and **DM-7MIT** in cyclohexane are shown in **Figure 2** and the corresponding photophysical data are summarized in **Table 1**. **DM-7HIT** showed two lower lying absorption bands with maxima at 310 nm (1.27 x 10^4 $M^{-1}cm^{-1}$) and 380 nm (3.52 x 10^3 $M^{-1}cm^{-1}$). Upon excitation under a standard air atmosphere, weak dual emission bands with maxima at 550 nm and 685 nm were observed. The excitation spectra acquired at both emission wavelengths are identical, and they also resemble the absorption spectra (**Figure S28**), indicating that both emission bands originate from the same ground-state species. Remarkably, the quantum yields, Φ_{em} values, of both emission bands drastically increases from 0.02% to ~1.0% (more than 50-fold) upon degassing, confirming their natural triplet character that is quenched by O_2. Importantly, both the 550 nm and 685 nm emission bands undergo identical population decays in 1.1 μs in degassed cyclohexane (see **Figure 3a** and **Table 2**). Note that the rather low quantum yields for both phosphorescence bands can be attributed to the operation of energy gap law and the spin-forbidden nature of the T_1 to S_0 transition.[50] The former causes a significant decrease in quantum yield with decreasing emission energy gap due to the increase of the vibrational overlap between emitting and ground states, enhancing the radiationless deactivation. The latter causes an intrinsic long radiative lifetime. As a result, other non-radiative pathways, e.g. vibrational relaxation or intersystem crossing, become competitive with the phosphorescence irradiation and suppresses the phosphorescence quantum efficiency.

To elucidate the emission and hence the photophysical properties, the -OH group of **DM-7HIT** was methylated, forming **DM-7MIT** (**Scheme 1**), which serves as a reference compound as it lacks the intramolecular H-bond. As shown in

Table 1. The photophysical data of the title compounds in cyclohexane at 298 K.

	Absorption		Emission		Q.Y.[a] (in %, aer./deg.)[b]
	λ_{cal} (nm)	λ_{exp} (nm)	λ_{cal} (nm)	λ_{exp} (nm)	
DM-7HIT	469,371	480, 378	607, 764	550, 685	0.02/1.0
DM-7MIT	580, 351	579, 353	369, 780	380, 690	1.0/1.0 for 380 0.02/0.43 for 690
DTDM-7HIT	464, 399	481, 403	633, 789	586, 703	0.04/0.24
DMADM-7HIT	468, 434	478,390	777	681	0.18/1.2

[a] **Q.Y. denotes quantum yield.** [a] **aer. and deg. stand for aeration in atmosphere and degas, respectively.**

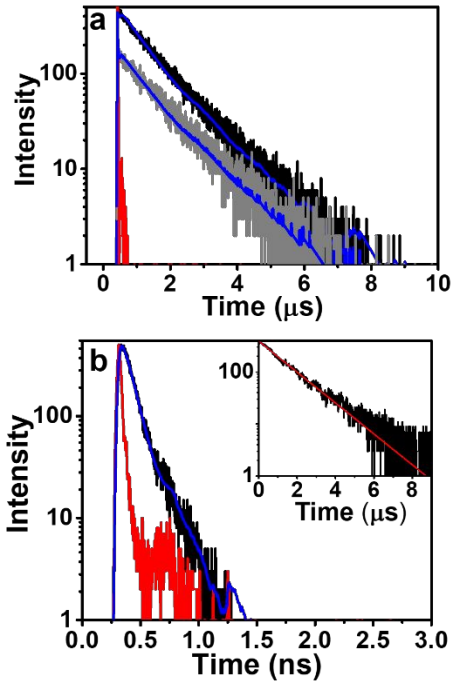

Figure 3. a, Microsecond time-resolved phosphorescence decays recorded for **DM-7HIT** (in degassed cyclohexane) monitored at 580 nm (black line) and 720 nm (grey line). The Instrument response time (IRF) is given by the red line. **b**, Pico-nanosecond time-resolved decays recorded for **DM-7MIT** monitored at 380 nm (black line). The IRF is given by the red line. Inset of **b**: The microsecond time-resolved emission decays recorded for **DM-7MIT** (in degassed cyclohexane) monitored at 700 nm.

Figure 2b, despite its absorption spectrum being similar to that of **DM-7HIT**, the emission spectrum of **DM-7MIT** is substantially different, and it shows dual emission bands with maxima at 380 nm and 690 nm. Upon degassing, also shown in **Figure 2b**, the quantum yield of the 690 nm emission band increases by a factor of approximately 28, whereas the intensity of the 380 nm emission band remains unchanged, implying that the 380 nm and 690 nm emission bands can be attributed to fluorescence and phosphorescence, respectively. This assignment is also supported by the time-resolved measurement, which showed that the lifetimes of the 380 nm and of 690 nm emission bands were 85 ps and as long as 1.5 μs, respectively, in degassed cyclohexane (see **Figure 3b** and **Table 2**).

The photophysics of thione-containing compounds have received considerable attention owing to the observation of $S_2 \rightarrow S_0$ fluorescence,[46-49] which is mainly due to the rather small ionization energy of the thione non-bonding orbital (n). As a result, the lowest lying excited state is attributed to an $n \rightarrow \pi^*$ transition, which is optically forbidden because of the orthogonality of the n and π^* orbitals. For **DM-7MIT**, this is evidenced by its very weak $S_0 \rightarrow S_1(n\pi^*)$ absorption maxima at ~580 nm with an absorption extinction coefficient as low as ε_{580} ~10 $M^{-1}cm^{-1}$ (see inset of **Figure 2b**). Conversely, the higher lying S_2 state mainly possesses $\pi\pi^*$ character at ~353 nm (ε_{350} ~4×10^3 $M^{-1}cm^{-1}$). The energy gap between $S_2(\pi\pi^*)$ and $S_1(n\pi^*)$ was calculated to be as large as ~11,057 cm^{-1}. This, together with their distinct orbital configurations, leads to anomalously slow $S_2(\pi\pi^*) \rightarrow S_1(n\pi^*)$ internal conversion, allowing the $S_2(\pi\pi^*) \rightarrow S_0$

Table 2. The time-resolved data of DM-7HIT and DM-7MIT in cyclohexane at 298 K.

	λ_{mon}/nm	τ_{exp}/ns recorded by TCSPC	τ_{exp}/ps (pre-factor) recorded by up-conversion
DM-7HIT	580	1100	0.3 (0.45), 3.4 (0.55)
	720	0.02[a] (0.91), 1100 (0.09)	0.3 (-0.5), 3.4 (0.5)
DM-7MIT	380	0.085	
	690	1460	

[a] lower than the instrument limit

radiative transition to be competitive. It is thus reasonable to assign the 380 nm band with a lifetime of 85 ps to the $S_2(\pi\pi^*) \rightarrow S_0$ fluorescence. This $S_2 \rightarrow S_0$ emission is deemed an exception to Kasha's rule, suggesting that the emission of the polyatomic molecules in the condensed phase is mostly from the lowest lying excited state.[51,] Similar assignments have been reported for a congener of **DM-7MIT**, 2,2-dimethyl-2,3-dihydro-*1H*-indene-1-thione (**DMIT**, **Figure S29**), which exhibited dual emission bands with maxima at 401 nm and 630 nm that were assigned to S_2 ($\pi\pi^*$) $\rightarrow S_0$ fluorescence and $T_1(n\pi^*) \rightarrow S_0$ phosphorescence, respectively.[46] Due to the lack of H-bond, the origin of the emission of **DM-7MIT** is expected to be the same as that of **DMIT**, which allows the 690 nm band of **DM-7MIT** to be reasonably assigned to the $T_1(n\pi^*) \rightarrow S_0$ phosphorescence.

In comparison, one of the obvious differences between **DM-7HIT** and **DM-7MIT** lies in the lack of observable $S_2(\pi\pi^*) \rightarrow S_0$ fluorescence for **DM-7HIT**. Shown in the inset of **Figure 2a**,

the weak $S_1(n\pi^*)$ absorption of **DM-7HIT** is located at 480 nm and has an onset at 530 nm, which is substantially blue shifted relative to $S_1(n\pi^*)$ of **DM-7MIT** (onset at ~650 nm). The results confirm the formation of the sulfur H-bond in **DM-7HIT**, and the thione lone-pair electrons are stabilized by the H-bond. Because the intramolecular H-bond has a slight influence on the π^* orbital, a significant increase in the $n \rightarrow \pi^*$ energy gap for **DM-7HIT** is observed (cf. **DM-7MIT**). Based on the $S_0 \rightarrow S_2(\pi\pi^*)$ (~380 nm) and $S_0 \rightarrow S_1(n\pi^*)$ (~480 nm) absorption maxima for **DM-7HIT**, the S_2-S_1 gap was calculated to be ~5,482 cm^{-1}, which is half the energy gap (~11,057 cm^{-1}) of **DM-7MIT**. The small energy gap leads to an ultrafast $S_2 \rightarrow S_1$ internal conversion, and the high rate of this internal conversion explains the lack of $S_2 \rightarrow S_0$ emission in **DM-7HIT**.

Another key difference lies in the observation of dual RT phosphorescence bands in **DM-7HIT** instead of the single phosphorescence band observed in **DM-7MIT**. We have made many efforts to explain this difference. One possibility is to assign the 550 and 685 nm phosphorescence bands to the T_1 and T_2 phosphorescence emissions, respectively. However, fundamentally, the ~10 kcal/mol separation in the energy gap between the 550 and 685 nm emission bands should lead to an ultrafast $T_2 \rightarrow T_1$ internal conversion via a vibrational relaxation, i.e., an internal conversion. Moreover, this mechanism cannot explain the identical phosphorescence decay time constants (1.1 μs) for the 550 and 685 nm emission bands and can thus be discarded. Another possible mechanism is the assignment of the 550 and 685 nm emission bands to fluorescence $S_1(n\pi^*)$ and phosphorescence ($T_1(n\pi^*$ or $\pi\pi^*)$). In this case, the $T_1 \rightarrow S_1(n\pi^*)$ reverse intersystem crossing has to be thermally accessible, so the $S_1(n\pi^*)$ 550 nm emission essentially exhibits a thermally activated delayed fluorescence to account for its population decay time constant (1.1 μs) being identical to that of the 685 nm T_1 phosphorescence. However, the T_1-S_1 energy gap being as large as 10 kcal/mol makes the reverse intersystem crossing strictly inaccessible at room temperature. This proposed mechanism can therefore be eliminated as well. We also considered the possibility that the 550 nm band is delayed fluorescence from T-T annihilation. If so, the ratio of the intensities of the 550 nm and 685 nm emission bands should be dependent on the excitation intensity. Conversely, the results show excitation-intensity independent ratiometric emissions (**Figure S30**). In addition, if the 550 nm delayed fluorescence originated from T-T annihilation, according to the kinetic expression, the relaxation decay time constant should be half of that of the 685 nm emission decay.[52] The equal decay time constants of the 550 nm and 680 nm emission bands also exclude the T-T annihilation mechanism.

The existence of an intramolecular H-bond in **DM-7HIT** is also reminiscent of the possibility of incorporating ESIPT via –OH-----S=C hydrogen bond, forming a C=O------H-S-C proton transfer tautomer (**Scheme S1**). Accordingly, the 550 nm and 680 nm bands of **DM-7HIT** can be assigned to the normal and proton-transfer tautomer phosphorescence, respectively, originating from ESIPT. In this case, we also have to assume that both the normal and proton-transfer tautomeric triplet states have similar energies such that a fast equilibrium takes place between the normal and tautomer triplet states to rationalize the identical decay rate constants. However, in-depth theoretical and experimental approaches raise serious concerns about this proposal. Theoretically, the time-dependent density functional theory (TD-DFT) approach at the B3LYP/6-311++G(3df,3pd) level for **DM-7HIT** in cyclohexane estimates that the energy of the tautomer S_1 ($\pi\pi^*$) state is higher than that of the normal species ($S_1(n\pi^*)$) by as much as 0.74 eV (~ 17 kcal/mol, **Scheme S1** and **Table S6**). In addition, the lowest triplet state of the proton-transfer tautomer, which was calculated to be T_1 ($\pi\pi^*$), is higher in energy than the lowest normal ($T_1(n\pi^*)$) state by at least 2.3 kcal/mol (see **Figure S31** and **Table S 7-9** for details of the state assignments). Although the calculated values are subject to uncertainty and the data should be varied by using different functionals and basis sets (**Table S 7-9**), we found that the trend in the thermally disfavoured ESIPT holds in both the singlet and triplet manifolds.

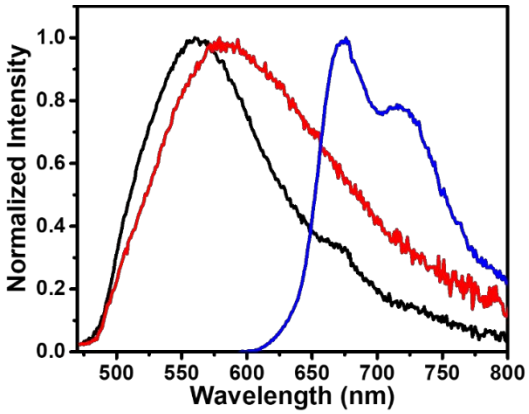

Figure 4. The phosphorescence spectra of **DM-7HIT** in a polyethylene film (black) at 298K and in the solid state (red) at 273K and **DM-7MIT** in solid state (blue) at 298K. λ_{ex}=405 nm and 360 nm for **DM-7HIT** and **DM-7MIT**, respectively.

Moreover, various experimental results cannot be explained based on ESIPT. First, in the pure solid at 0 °C (melting point 10 °C for **DM-7HIT**), **DM-7HIT** showed only one phosphorescence band with a maximum at ~590 nm (τ_{obs} ~4.2 μs, **Figure 4**). Similarly, rigid polyethylene (PE) doped with **DM-7HIT** revealed only one phosphorescence band at ~595 nm (τ_{obs} ~ 1.3 μs). Because the occurrence of ESIPT requires only a slight shift in the proton along the existing H-bond, the absence of the purported proton-transfer tautomer emission, i.e., the 685 nm band, cannot be rationalized by the inhibition of ESIPT in the solid state or in a solid matrix unless **DM-7HIT** lacks the intramolecular H-bond in solid environment. However, the intramolecular H-bond formation in the solid crystal is supported by the X-ray structure of **7HIT**. Additionally, the emission spectrum of the O-H deuterated **DM-7DIT** in cyclohexane is identical with that of the non-deuterated **DM-7HIT** (the green dashed line in **Figure 2**), affirming that the lack of O-D deuterium isotope effect in its photophycial behavior. This observation, in an indirect manner, also devaluates the possibility of ESIPT. Therefore, both the theoretical and experimental approaches disapprove the ESIPT mechanism.

The proposed H-bond on/off mechanism We also estimated the O-H----S hydrogen bond energy by calculating the energy difference between **DM-7HIT** with a H-bond and **DM-7HIT** without a H-bond. The latter was done by initially locating the H atom at the site opposite the H-bond and optimizing the system to find a local minimum. As a result, an intramolecular H-bond stabilizes **DM-7HIT** by 9.8 kcal/mol (B3LYP/6-311++G(3df,3pd), **Figure 5a** and **Scheme S1**), and this should be the dominant species in the ground state, which

would be consistent with the ^{1}H NMR spectra (*vide supra*). However, upon excitation of the lowest lying n → π* transition, the electron density in the thione non-bonding (n) orbital decreases, shown in **Figure 5b**, which substantially reduces the proton-accepting strength of the sulfur and hence weakens the H-bond. Therefore, as for the phosphorescence of **DM-7HIT**, the corresponding emitting state may no longer only be the intramolecular H-bonded $T_1(n\pi^*)$ state. This mechanism is supported by the computational result indicating that the H-bonded $T_1(n\pi^*)$ state of **DM-7HIT** is only 1.7 kcal/mol higher in energy than that of the non-H-bonded $T'_1(n\pi^*)$ (herein, prime indicates the non-H-bonded species) states

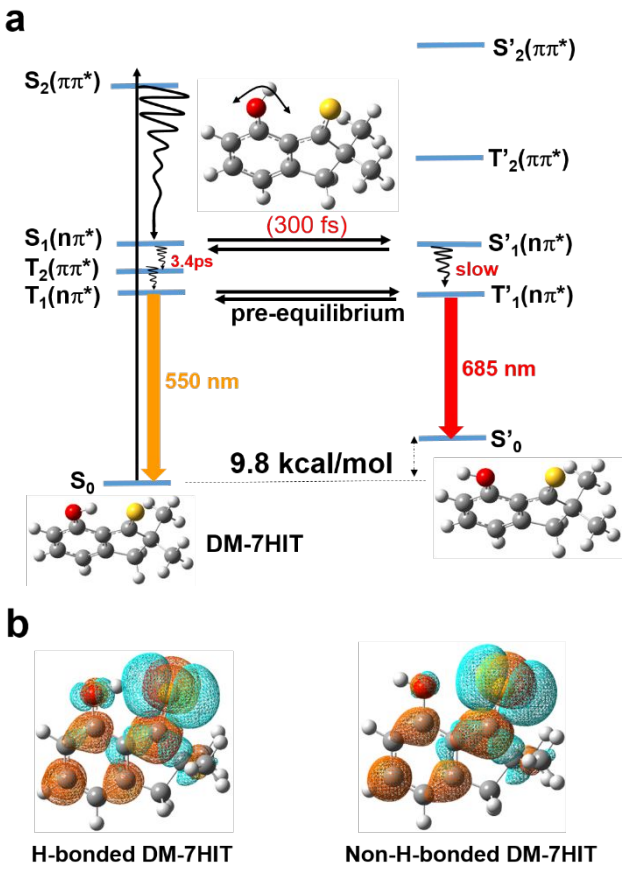

Figure 5. a, The schematic energy diagram of the mechanism of H-bonding hopping for **DM-7HIT**. The energy gaps between the corresponding states of the H-bonded and the non-H-bonded forms are calculated values and the emission wavelengths were taken from the observed maxima. An animation of the H-bond flipping is provided as a supplementary video. **b,** The calculated HOMO (cyan color) and LUMO (orange color) of H-bonded and non-H-bonded **DM-7HIT**.

in cyclohexane. Considering the uncertainty of the current computational approach, it is reasonable to expect a thermal equilibrium between $T_1(n\pi^*)$ and $T'_1(n\pi^*)$ in a nonpolar solution. Additionally, the difference in the emission peaks (550 and 685 nm) was calculated to be ~10 kcal/mol, which is consistent with the calculated difference between the H-bonded S_0 and non-H-bonded S'_0 species (9.8 kcal/mol, *vide supra*). Moreover, based on total energy differences, the calculations showed that the vertical transitions of $T_1(n\pi^*) \rightarrow S_0$ and $T'_1(n\pi^*) \rightarrow S'_0$ occur at 607 nm and 764 nm, respectively, which are in good agreement with the observed dual phosphorescence peaks (**Table S10**). When the angle of O-H---S was gradually varied from $T_1(n\pi^*)$ to a local minimum $T'_1(n\pi^*)$, we estimated the barrier of the $T_1(n\pi^*) \rightarrow T'_1(n\pi^*)$ H-bond on/off flipping to be as small as ~1.0 kcal/mol (**Figure S32**).

Based on these analyses, we thus propose the most acceptable mechanism incorporating a fast pre-equilibrium between the $T_1(n\pi^*)$ and $T'_1(n\pi^*)$ states, which is essentially an intramolecular H-bond on/off switching process, exhibiting solution-phase RTPs of 550 nm and 685 nm with identical decay time constants (*vide supra*). The above H-bond flipping mechanism is supported by the fact that the 685 nm phosphorescence of **DM-7HIT** with the vibronic spectral feature is nearly identical to that of the phosphorescence of **DM-7MIT,** which lacks H-bond (**Figure 2a**, **b**). Additionally, this mechanism rationalizes the observation of a single phosphorescence band in the solid crystal and PE film, which, according to the mechanism, can be attributed to the H-bonded $T_1(n\pi^*)$ emission because of the inhibition of –OH flipping to the $T'_1(n\pi^*)$ state by the solid matrix. We also carried out the steady-state spectra of **DM-7HIT** in different solvents and the results are shown in **Figure S33**. With increasing solvent polarity, the non-H-bonded emission becomes predominant. This phenomenon, driven by the stabilization of hydroxyl group of non-H-bonded species by polar solvent molecules, also supports the proposed mechanism of H-bond flipping. Remarkably, the S_2 emission can also be observed in methanol due to the external H-bonds with methanol molecules, which makes the non-H-bonded species (S'_0 in **Figure 5a**) partially exist in ground state.

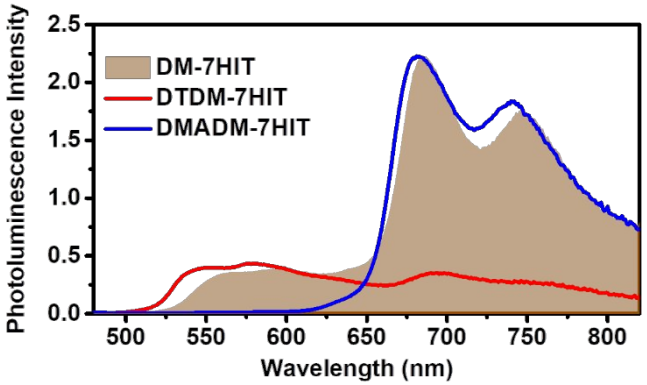

Figure 6. Comparison of the emission spectra of **DM-7HIT** (orange filled area), **DTDM-7HIT** (red) and **DMADM-7HIT** (blue) in cyclohexane at room temperature. λ_{ex}: 380 nm.

The strategic design and synthesis of **DTDM-7HIT** (see **Figure S5** for X-ray structure) and **DMADM-7HIT** (**Scheme 1**) further supported the proposed mechanism. **DTDM-7HIT** is the derivative of **DM-7HIT** with a *tert*-butyl substituent at the *ortho* (C6) and *para* (C4) position. Chemically, we expect that the population of non-H-bonded species in the triplet state will be suppressed (cf. the H-bonded species) due to steric hindrance from the bulky *tert*-butyl group at C6, which decreases the degrees of freedom of the non-H-bonded species. Supportively, the **DTDM-7HIT** in cyclohexane (**Figure 6** and **Figure S34**) showed a dramatic decrease in the 685 nm $T'_1(n\pi^*)$ phosphorescence relative to that of **DM-7HIT** (**Figure 2a**).

In yet another approach, for **DMADM-7HIT**, which is synthesized by inserting a dimethylaminomethyl moiety *ortho*

to the hydroxyl group of **DM-7HIT** via a Mannich reaction (**Scheme 1**), formation of an O-H-----N H-bond is competitive with O-H-----S H-bond formation (**Figure 7**). Nevertheless, the computational studies indicate that the **DMADM-7HIT** conformer having the O-H-----S H-bond is more stable than the O-H-----N H-bonded conformer by 2.65 kcal/mol and is the dominant species in the ground state. This is also evidenced experimentally by **DMADM-7HIT** and **DM-7HIT** having the same $S_0 \rightarrow S_1(n\pi^*)$ absorption at 530 nm (**Figure S34** and **Figure 2a**). However, despite O-H-----S H-bonded **DMADM-7HIT** being the dominant species in the ground state, upon excitation, only the 681 nm phosphorescence peak belonging to the non-O-H-----S H-bonded form can be observed (**Figure 6**). The absence of the 550 nm phosphorescence peak corresponding to

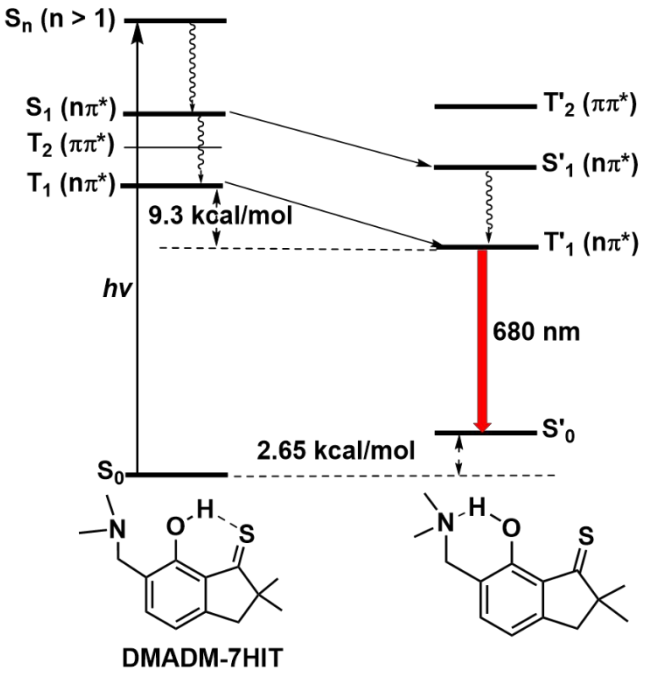

Figure 7. The schematic energy diagram of the mechanism of H-bonding hopping in **DMADM-7HIT**. The energy gaps between the corresponding states of the H-bonded and the non-H-bonded forms are calculated values, and the emissions in wavelengths are taken from the observed peak wavelengths.

the O-H-----S H-bonded form indicates that in the triplet emitting state of **DMADM-7HIT**, the equilibrium shifts completely to the O-H----N H-bonded species because of the much weaker O-H-----S H-bond in the $T_1(n\pi^*)$ state. This phenomenon is further supported by the computational studies involving the optimization of the geometry of both the O-H----N and O-H-----S H-bond species under the nπ* configuration, and these studies concluded that the O-H-----N H-bonded $T'_1(n\pi^*)$ state is more stable than the O-H-----S H-bonded $T_1(n\pi^*)$ state by 9.3 kcal/mol (see **Figure 7**).

The substituent effect on triplet stabilization can be more clearly seen from computational approach shown in **Figure S32**. Compared to **DM-7HIT**, the $T'_1(n\pi^*)$ state of the **DMADM-7HIT** is significantly lowered due to the O-H-----N stabilization, whereas the incorporation of a bulky tert-butyl group (**DTDM-7HIT**) raises the energy of the $T'_1(n\pi^*)$ state of the H-flipping product due to the steric repulsion. The nπ* triplet excited states before and after the H flipping, involving an almost negligible small rotation barrier, have nearly the same energy for **DTDM-7HIT**. The theoretically predicted near 1:1 thermodynamic population for the two triplet excited states corresponds to the much more evenly distributed emission intensities of the two phosphorescent bands for **DTDM-7HIT**, shown in **Figure 6.** These results provide indisputable evidence to support the H-bond flipping mechanism established in **DM-7HIT**.

Based on the above analyses, we then measured the initial relaxation kinetics to elucidate the corresponding H-bond flipping dynamics of **DM-7HIT**. To avoid any additional relaxation processes, the excitation wavelength was tuned to 400 nm, which is near the onsetof the $S_0 \rightarrow S_2$ ($\pi\pi^*$) absorption adjacent to the $S_0 \rightarrow S_1(n\pi^*)$ transition (inset of **Figure 2a**.). First, we used time-correlated single-photon counting (TCSPC) measurements with a femtosecond laser source (180 fs, 1 kHz repetition rate) and a multichannel plate as the detector. After convolution, the system response was estimated to be ~25 ps. However, as shown in **Figure S37**, the results indicated that both the 550 and 685 nm emission bands consist of an ultrafast early decay component that is beyond the system response (< 25 ps). To gain further insight into the dynamics of the H-bond flipping, we then applied a femtosecond up-conversion technique, and the results are shown in **Figure 8** with the pertinent time-resolved data presented in **Table 2**.

When monitoring at an emission wavelength of 580 nm, two decay components were observed in a 10 ps window, and the components were fitted to be 0.3 ps and 3.4 ps. Notably, the phosphorescence decay components that appear in **Figure 8** cannot be resolved in this time regime because they are forbidden and hence their initial

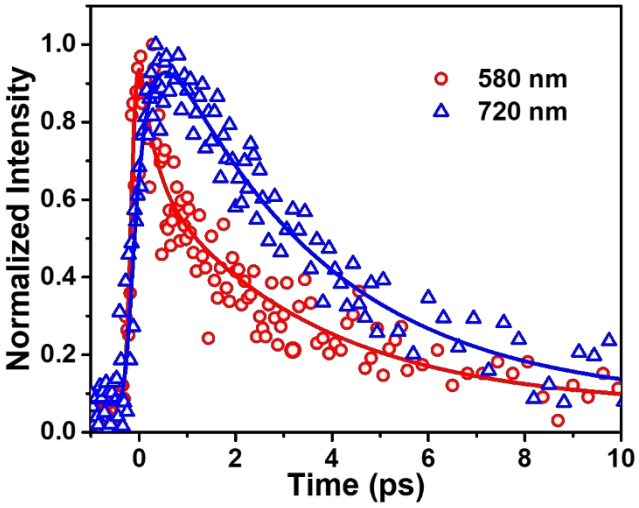

Figure 8. The early dynamics decay curve of **DM-7HIT** at 550 nm (blue) and 740 nm (red).

intensities are rather low. Upon monitoring at 720 nm, a rise component of 0.3 ps followed by a 3.4 ps decay can be observed. The results reveal precursor-successor-type kinetic behaviour under a thermal equilibrium.[53-55] These results, together with the microsecond time-resolved data (**Figure 3a**), are sufficient to understand the relaxation dynamics behind the dual RTP signals. The lowest lying excited state (S_1) for **DM-7HIT** is a sulfur non-bonding (n) → π* transition, which drastically weakens the O-H----S H-bond and results in fast O-H bond flipping from $S_1(n\pi^*)$ to a non-H-bonded $S'_1(n\pi^*)$ state

with a ~300 fs time constant, which is of the same magnitude as the torsional motion. Similar to the equilibrium observed between the $T_1(n\pi^*)$ and $T'_1(n\pi^*)$ states, it is also reasonable to expect thermal interconversion between the $S'_1(n\pi^*)$ and $S_1(n\pi^*)$ states, which give the same decay time of 3.4 ps. Based on the computational studies, the energy of $T_2(\pi\pi^*)$ state is in between those of the $S_1(n\pi^*)$ and $T_1(n\pi^*)$ states (**Figure 5**). Therefore, the flipping of the n → π* orbital should greatly enhance the rate of $S_1(n\pi^*) \rightarrow T_2(\pi\pi^*)$ intersystem crossing,[56] rationalizing the fast 3.4 ps decay time constant.[57-59] This is also supported by the calculated spin-orbit coupling (SOC) integral of 32 cm^{-1} between the $S_1(n\pi^*)$ and $T_2(\pi\pi^*)$ states, which is much larger than that between $S(n\pi^*)$ and $T(n\pi^*)$ states calculated in previous report.[57] (see experimental in **SI**) Prior to the decay of either the $T'_1(n\pi^*)$ or $T_1(n\pi^*)$ state, fast H-bond on/off switch occurs between $T'_1(n\pi^*)$ and $T_1(n\pi^*)$ in a pre-equilibrium, rendering dual $T'_1(n\pi^*$, 685 nm) and $T_1(n\pi^*$, 550 nm) RTP with the identical phosphorescence lifetime.

CONCLUSION

In summary, we have presented a seminal study on a photoinduced intramolecular H-bond on/off reaction along a pre-existing sulfur H-bond. The flipping of the H-bond in the nπ* state originates from the n → π* transition, causing an electron deficiency in the non-bonding orbital of the S atom and hence drastically reducing its proton-accepting strength and weakening the H-bond. This photoinduced H-bond on/off reaction should be universal for molecules having an nπ* configuration for their lowest lying excited state, in which the non-bonding (n) orbital is involved in the H-bond. Thione-type H-bonds are an example of such species because of thione's low electron binding energy and hence lower ionization energy for the non-bonding electron, making this phenomenon applicable to many of the other thiobases that have recently been intensively studied due to their potential as artificial DNA/RNA bases and formation of hydrogen bonding pair[57, 60-61]. Nevertheless, this is not believed to be a unique case. Small organic molecules possessing carbonyl groups that serve as proton acceptors to form intramolecular or intermolecular H-bonds may have an nπ* configuration as the lowest state, and these molecules would therefore be expected to undergo similar H-bonding on/off flipping phenomena. Overall, the H-bonding on-off flipping creates two excited-state isomers that may have drastically different photophysical properties, as evidenced by the thiones studied above; thus, this represents previously unrecognized photochemistry. The photoinduced H-bonding on/off flipping and the resulting dual room-temperature phosphorescence of the sulfur-containing intramolecular H-bonds may thus open a new chapter in the chemistry of hydrogen bonds.

ASSOCIATED CONTENT

The **Supporting Information** is available free of charge via the Internet at http://pubs.acs.org.
Details of synthetic procedures, characterization, computational approach, photophysical measurements (PDF)
Hydrogen bond flipping animation (MP4)

AUTHOR INFORMATION

Corresponding Author

Pi-Tai Chou, e-mail: chop@ntu.edu.tw
Kew-Yu Chen, e-mail: kyuchen@fcu.edu.tw
Elise Y. Li, e-mail: eliseytli@ntnu.edu.tw

Author Contributions

Z.-Y. Liu, J.-W. Hu, C.-H. Huang contributed equally.

ACKNOWLEDGMENT

We appreciate the Ministry of Science and Technology (MOST 107-2628-M-002-017, MOST 107-2113-M-035 -003, and MOST 106-2113-M-003-010-MY3), Taiwan, for their generous support.

REFERENCES

1. Copley, M. J.; Marvel, C. S.; Ginsberg, E., Hydrogen Bonding by S-H. Vll. Aryl Mercaptans. *J. Am. Chem. Soc.* **1939,** *61*, 3161-3162.
2. Gordy, W.; Stanford, S. C., Spectroscopic evidence for hydrogen bonds SH, NH and NH compounds. *J. Am. Chem. Soc.* **1940,** *62*, 497-505.
3. Heafield, T. G.; Hopkins, G.; Hunter, L., Hydrogen bonds involving the sulphur atom. *Nature* **1942,** *149*, 218-218.
4. González, L.; Mó, O.; Yáñez, M., High-level ab initio calculations on the intramolecular hydrogen bond in thiomalonaldehyde. *J. Phys. Chem. A* **1997,** *101*, 9710-9719.
5. Jabłoński, M.; Kaczmarek, A.; Sadlej, A. J., Estimates of the energy of intramolecular hydrogen bonds. *J. Phys. Chem. A* **2006,** *110*, 10890-10898.
6. Nowroozi, A.; Roohi, H.; Hajiabadi, H.; Raissi, H.; Khalilinia, E.; Birgan, M. N., O-H···S intramolecular hydrogen bond in thiomalonaldehyde derivatives; a quantum chemical study. *Comput. Theor. Chem.* **2011,** *963*, 517-524.
7. Posokhov, Y.; Gorski, A.; Spanget-Larsen, J.; Duus, F.; Hansen, P. E.; Waluk, J., The structure of the phototransformation product of monothiodibenzoylmethane. *Chem. Phys. Lett.* **2001,** *350*, 502-508.
8. Biswal, H. S.; Wategaonkar, S., Nature of the N-H···S Hydrogen Bond. *J. Phys. Chem. A* **2009,** *113*, 12763-12773.
9. Šponer, J.; Jurečka, P.; Hobza, P., Accurate interaction energies of hydrogen-bonded nucleic acid base pairs. *J. Am. Chem. Soc.* **2004,** *126*, 10142-10151.
10. Villalobos, A.; Ness, J. E.; Gustafsson, C.; Minshull, J.; Govindarajan, S., Gene Designer: a synthetic biology tool for constructing artificial DNA segments. *Bmc Bioinformatics* **2006,** *7*.
11. Kumar, D.; Gustafsson, C.; Klessig, D. F., Validation of RNAi silencing specificity using synthetic genes: salicylic acid-binding protein 2 is required for innate immunity in plants. *Plant J.* **2006,** *45*, 863-868.
12. Gustafsson, C.; Govindarajan, S.; Minshull, J., Putting engineering back into protein engineering: bioinformatic approaches to catalyst design. *Curr. Opin. Biotechnol.* **2003,** *14*, 366-370.
13. Yanagisawa, Y.; Nan, Y. L.; Okuro, K.; Aida, T., Mechanically robust, readily repairable polymers via tailored noncovalent cross-linking. *Science* **2018,** *359*, 72-+.
14. Biswal, H. S.; Wategaonkar, S., Sulfur, Not Too Far Behind O, N, and C: SH···π Hydrogen Bond. *J. Phys. Chem. A* **2009,** *113*, 12774-12782.
15. Saggu, M.; Levinson, N. M.; Boxer, S. G., Direct Measurements of Electric Fields in Weak OH-π Hydrogen Bonds. *J. Am. Chem. Soc.* **2011,** *133*, 17414-17419.
16. Saggu, M.; Levinson, N. M.; Boxer, S. G., Experimental Quantification of Electrostatics in X-H···π Hydrogen Bonds. *J. Am. Chem. Soc.* **2012,** *134*, 18986-18997.
17. Shchavlev, A. E.; Pankratov, A. N.; Shalabay, A. V., Theoretical studies on the intramolecular hydrogen bond and tautomerism of 8-mercaptoquinoline in the gaseous phase and in solution using modern DFT methods. *J. Phys. Chem. A* **2005,** *109*, 4137-4148.

18. González, L.; Mó, O.; Yáñez, M., Substituent effects on the strength of the intramolecular hydrogen bond of thiomalonaldehyde. *J. Org. Chem.* **1999,** *64*, 2314-2321.

19. Schaefer, T.; Salman, S. R.; Wildman, T. A.; Clark, P. D., Conformational Consequences of Intramolecular Hydrogen-Bonding by Oh to the Directional Lone-Pair of Sulfur in Derivatives of Methyl Phenyl Sulfide, Diphenyl Sulfide, and Diphenyl Disulfide. *Can. J. Chem.* **1982,** *60*, 342-348.

20. Szmant, H. H.; Rigau, J. J., Intramolecular Hydrogen Bonding in Cis-2-Phenylmercaptoindanol. *J. Org. Chem.* **1966,** *31*, 2288-+.

21. Mundlapati, V. R.; Gautam, S.; Sahoo, D. K.; Ghosh, A.; Biswal, H. S., Thioamide, a Hydrogen Bond Acceptor in Proteins and Nucleic Acids. *J. Phys. Chem. Lett.* **2017,** *8*, 4573-4579.

22. Adhikari, U.; Scheiner, S., Contributions of Various Noncovalent Bonds to the Interaction between an Amide and S-Containing Molecules. *Chemphyschem* **2012,** *13*, 3535-3541.

23. Meyer, E. A.; Castellano, R. K.; Diederich, F., Interactions with aromatic rings in chemical and biological recognition. *Angew. Chem. Int. Ed.* **2003,** *42*, 1210-1250.

24. Salonen, L. M.; Ellermann, M.; Diederich, F., Aromatic Rings in Chemical and Biological Recognition: Energetics and Structures. *Angew. Chem. Int. Ed.* **2011,** *50*, 4808-4842.

25. Steiner, T.; Koellner, G., Hydrogen bonds with π-acceptors in proteins: Frequencies and role in stabilizing local 3D structures. *J. Mol. Biol.* **2001,** *305*, 535-557.

26. Barbara, P. F.; Brus, L. E.; Rentzepis, P. M., Intramolecular Proton-Transfer and Excited-State Relaxation in 2-(2-Hydroxyphenyl)Benzothiazole. *J. Am. Chem. Soc.* **1980,** *102*, 5631-5635.

27. Beens, H.; Grellman.Kh; Gurr, M.; Weller, A. H., Effect of Solvent and Temperature on Proton Transfer Reactions of Excited Molecules. *Discuss. Faraday Soc.* **1965**, 183-193.

28. Mcmorrow, D.; Kasha, M., Intramolecular Excited-State Proton-Transfer in 3-Hydroxyflavone - Hydrogen-Bonding Solvent Perturbations. *J. Phys. Chem.* **1984,** *88*, 2235-2243.

29. Williams, D. L.; Heller, A., Intramolecular Proton Transfer Reactions in Excited Fluorescent Compounds. *J. Phys. Chem.* **1970,** *74*, 4473-4480.

30. Lin, W. C.; Fang, S. K.; Hu, J. W.; Tsai, H. Y.; Chen, K. Y., Ratiometric Fluorescent/Colorimetric Cyanide-Selective Sensor Based on Excited-State Intramolecular Charge Transfer-Excited-State Intramolecular Proton Transfer Switching. *Anal. Chem.* **2014,** *86*, 4648-4652.

31. Xu, Y. Q.; Pang, Y., Zn^{2+}-triggered excited-state intramolecular proton transfer: a sensitive probe with near-infrared emission from bis(benzoxazole) derivative. *Dalton Trans.* **2011,** *40*, 1503-1509.

32. Yu, L.; Li, Y. Y.; Yu, H.; Zhang, K.; Wang, X. W.; Chen, X. F.; Yue, J.; Huo, T. X.; Ge, H. W.; Alamry, K. A.; Marwani, H. M.; Wang, S. H., A fluorescence probe for highly selective and sensitive detection of gaseous ozone based on excited-state intramolecular proton transfer mechanism. *Sens. Actuat. B-Chem.* **2018,** *266*, 717-723.

33. Maity, D.; Kumar, V.; Govindaraju, T., Reactive Probes for Ratiometric Detection of Co^{2+} and Cu^{+} Based on Excited-State Intramolecular Proton Transfer Mechanism. *Org. Lett.* **2012,** *14*, 6008-6011.

34. Sytnik, A.; Gormin, D.; Kasha, M., Interplay between Excited-State Intramolecular Proton-Transfer and Charge-Transfer in Flavonols and Their Use as Protein-Binding-Site Fluorescence Probes. *Proc. Natl. Acad. Sci. USA* **1994,** *91*, 11968-11972.

35. Sytnik, A.; Kasha, M., Excited-State Intramolecular Proton-Transfer as a Fluorescence Probe for Protein Binding-Site Static Polarity. *Proc. Natl. Acad. Sci. USA* **1994,** *91*, 10757-10757.

36. Chen, K. Y.; Hsieh, C. C.; Cheng, Y. M.; Lai, C. H.; Chou, P. T., Extensive spectral tuning of the proton transfer emission from 550 to 675 nm via a rational derivatization of 10-hydroxybenzo[h]quinoline. *Chem. Commun.* **2006**, 4395-4397.

37. Hsu, Y. H.; Chen, Y. A.; Tseng, H. W.; Zhang, Z. Y.; Shen, J. Y.; Chuang, W. T.; Lin, T. C.; Lee, C. S.; Hung, W. Y.; Hong, B. C.; Liu, S. H.; Chou, P. T., Locked ortho- and para-Core Chromophores of Green Fluorescent Protein; Dramatic Emission Enhancement via Structural Constraint. *J. Am. Chem. Soc.* **2014,** *136*, 11805-11812.

38. Park, S.; Kwon, O. H.; Kim, S.; Park, S.; Choi, M. G.; Cha, M.; Park, S. Y.; Jang, D. J., Imidazole-based excited-state intramolecular proton-transfer materials: Synthesis and amplified spontaneous emission from a large single crystal. *J. Am. Chem. Soc.* **2005,** *127*, 10070-10074.

39. Mamada, M.; Inada, K.; Komino, T.; Potscavage, W. J.; Nakanotani, H.; Adachi, C., Highly Efficient Thermally Activated Delayed Fluorescence from an Excited-State Intramolecular Proton Transfer System. *ACS Central. Sci.* **2017,** *3*, 769-777.

40. Park, S.; Seo, J.; Kim, S. H.; Park, S. Y., Tetraphenylimidazole-based excited-state intramolecular proton-transfer molecules for highly efficient blue electroluminescence. *Adv. Funct. Mater.* **2008,** *18*, 726-731.

41. Tang, K. C.; Chang, M. J.; Lin, T. Y.; Pan, H. A.; Fang, T. C.; Chen, K. Y.; Hung, W. Y.; Hsu, Y. H.; Chou, P. T., Fine Tuning the Energetics of Excited-State Intramolecular Proton Transfer (ESIPT): White Light Generation in A Single ESIPT System. *J. Am. Chem. Soc.* **2011,** *133*, 17738-17745.

42. Pedersen, B. S.; Scheibye, S.; Nilsson, N. H.; Lawesson, S. O., Studies on Organophosphorus Compounds XX. Syntheses of Thioketones. *Bull. Soc. Chim. Belg.* **1978,** *87*, 223-228.

43. Scheibye, S.; Shabana, R.; Lawesson, S. O.; Rømming, C., Studies on Organo-Phosphorus Compounds-XL: Reactions of Ketones with 2,4-Bis(4-Methoxyphenyl)-1,3,2,4-Dithiadiphosphetane 2,4-Disulfide. *Tetrahedron* **1982,** *38*, 993-1001.

44. Rufanov, K. A.; Stepanov, A. S.; Lemenovskii, D. A.; Churakov, A. V., Synthesis and structure of anhydroindanone-1 disulfide. *Heteroat. Chem.* **1999,** *10*, 369-371.

45. Böhlig, H.; Ackermann, M.; Billes, F.; Kudra, M., Vibrational analysis of benzothiazoline-2-thione. *Spectrochim Acta A* **1999,** *55*, 2635-2646.

46. Evans, R. C.; Douglas, P.; Winscom, C. J., Photophysics and Electrochemistry of some Thione Far-Red/Near-IR Triplet Emitters. *J. Fluoresc.* **2009,** *19*, 169-177.

47. Maciejewski, A.; Steer, R. P., The Photophysics, Physical Photochemistry, and Related Spectroscopy of Thiocarbonyls. *Chem. Rev.* **1993,** *93*, 67-98.

48. Steer, R. P.; Ramamurthy, V., Photophysics and Intramolecular Photochemistry of Thiones in Solution. *Acc. Chem. Res.* **1988,** *21*, 380-386.

49. Maciejewski, A.; Szymanski, M.; Steer, R. P., T_1-T_2 Inversion in Aromatic Thiones. *Chem. Phys. Lett.* **1988,** *143*, 559-564.

50. Englman, R.; Jortner, J., The energy gap law for radiationless transitions in large molecules. *Mol. Phys.* **1970,** *18*, 145-164.

51. Demchenko, A. P.; Tomin, V. I.; Chou, P. T., Breaking the Kasha Rule for More Efficient Photochemistry. *Chem. Rev.* **2017,** *117*, 13353-13381.

52. Wu, P. C.; Yu, J. K.; Song, Y. H.; Chi, Y.; Chou, P. T.; Peng, S. M.; Lee, G. H., Synthesis and characterization of metal complexes possessing the 5-(2-pyridyl) pyrazolate ligands: The observation of remarkable osmium-induced blue phosphorescence in solution at room temperature. *Organometallics* **2003,** *22*, 4938-4946.

53. Shynkar, V. V.; Mély, Y.; Duportail, G.; Piémont, E.; Klymchenko, A. S.; Demchenko, A. P., Picosecond time-resolved fluorescence studies are consistent with reversible excited-state intramolecular proton transfer in 4 '-(dialkylaminoe)-3-hydroxyflavones. *J. Phys. Chem. A* **2003,** *107*, 9522-9529.

54. Zhou, C. K.; Tian, Y.; Yuan, Z.; Han, M. G.; Wang, J.; Zhu, L.; Tameh, M. S.; Huang, C.; Ma, B. W., Precise Design of Phosphorescent Molecular Butterflies with Tunable Photoinduced Structural Change and Dual Emission. *Angew. Chem. Int. Ed.* **2015,** *54*, 9591-9595.

55. Liu, Z. Y.; Hu, J. W.; Chen, C. L.; Chen, Y. A.; Chen, K. Y.; Chou, P. T., Correlation among Hydrogen Bond, Excited-State Intramolecular Proton-Transfer Kinetics and Thermodynamics for -OH Type Proton-Donor Molecules. *J. Phys. Chem. C* **2018,** *122*, 21833-21840.

56. Marian, C. M., Spin-orbit coupling and intersystem crossing in molecules. *Wires Comput. Mol. Sci.* **2012,** *2*, 187-203.

57. Borrego-Varillas, R.; Teles-Ferreira, D. C.; Nenov, A.; Conti, I.; Ganzer, L.; Manzoni, C.; Garavelli, M.; de Paula, A. M.; Cerullo, G., Observation of the Sub-100 Femtosecond Population of a Dark State in a Thiobase Mediating Intersystem Crossing. *J. Am. Chem. Soc.* **2018,** *140*, 16087-16093.

58. Mai, S.; Marquetand, P.; González, L., Intersystem Crossing Pathways in the Noncanonical Nucleobase 2-Thiouracil: A Time-Dependent Picture. *J. Phys. Chem. Lett.* **2016,** *7*, 1978-1983.

59. Reichardt, C.; Guo, C.; Crespo-Hernández, C. E., Excited-State Dynamics in 6-Thioguanosine from the Femtosecond to Microsecond Time Scale. *J. Phys. Chem. B* **2011,** *115*, 3263-3270.

60. Pollum, M.; Jockusch, S.; Crespo-Hernández, C. E., Increase in the photoreactivity of uracil derivatives by doubling thionation. *PCCP* **2015,** *17*, 27851-27861.

61. Karran, P.; Attard, N., Thiopurines in current medical practice: molecular mechanisms and contributions to therapy-related cancer. *Nat. Rev. Cancer* **2008,** *8*, 24-36.

Insert Table of Contents artwork here